On the uniqueness of structure extracted from diffraction experiments on liquids and glasses

2007 J. Phys.: Condens. Matter 19 415108

(http://iopscience.iop.org/0953-8984/19/41/415108)

IOP PUBLISHING JOURNAL OF PHYSICS: CONDENSED MATTER

J. Phys.: Condens. Matter **19** (2007) 415108 (15pp) doi:10.1088/0953-8984/19/41/415108

On the uniqueness of structure extracted from diffraction experiments on liquids and glasses

A K Soper

ISIS Facility, Science and Technology Facilities Council, Rutherford Appleton Laboratory, Harwell Science and Innovation Campus, Didcot, Oxon OX11 0QX, UK

Received 22 May 2007, in final form 1 July 2007
Published 27 September 2007
Online at stacks.iop.org/JPhysCM/19/415108

Abstract

There is continued interest in the problem of extracting structures from x-ray and neutron diffraction data on liquids and glasses. Traditional Fourier transform techniques, with their inherent weakness of possible systematic and truncation artefacts being introduced into the estimated distribution functions, are increasingly being complemented by computer simulation methods. These allow three-dimensional models of the scattering system to be built, at the correct atomic number density, which are consistent with both the diffraction data themselves and with other known or estimated constraints such minimum particle separations. Here the empirical potential structure refinement (EPSR) method is used to explore structure in supercooled liquid Ni, amorphous Ge and amorphous $GeSe_2$, and to evaluate alternative versions of the radial distribution functions which are consistent with the diffraction data. In the case of liquid Ni, it is found that there is, based on the diffraction data, some uncertainty on the hardness and shape of the repulsive core of the interatomic pair potential, and this may influence the current debate about the existence of icosahedral order in this liquid. For amorphous Ge two distinct radial distribution functions are generated, both consistent with the diffraction data, one of which has strong tetrahedral local order with the other having a predominantly triangular local coordination. For amorphous $GeSe_2$ it is found the SeSe and GeSe radial distribution functions can be determined well from the data, but the GeGe distribution is more uncertain, with the best fits implying both GeGe and SeSe homopolar bonds as originally proposed. The results are used to discuss the ambiguities inherent in the structural interpretation of diffraction data, even for one- and two-component systems.

(Some figures in this article are in colour only in the electronic version)

1. Introduction

Since the mid-1980s there has been an ongoing interest in finding ways of extracting more information from diffraction data beyond the traditional approach of simply performing a direct Fourier transform on the data to give the radial distribution function, $g(r)$. Initially methods

revolved around using $g(r)$ itself to generate an effective interatomic pair potential, which could in turn be used within a computer simulation of the material in question [1, 2] to estimate higher order correlation functions. Later [3] the reverse Monte Carlo (RMC) method was invented, which took a somewhat different tack in that it used the fit to the diffraction data to determine whether to accept or reject atom moves, rather than the interatomic potential of conventional simulation methods. The RMC method has been used extremely widely, with a significant degree of success, to interpret diffraction data from a broad range of monatomic and multicomponent liquids and glasses [4].

A number of variants of these different methods have emerged [5–7], and the present paper will use the last of these methods, empirical potential structure refinement (EPSR), to examine the question of how well we know the radial distribution functions for a liquid or glass based on a set of diffraction data. The study of this reliability issue can be achieved within EPSR by altering the so-called 'reference potential' which is used to seed the computer simulation. The reference potential is present in EPSR to build in prior knowledge, such as the likely minimum approach distances between atoms, the nature of likely local interactions (ionic bonding for example) and, if molecules are present, the known molecular geometries. By changing the reference potential one can build in different assumptions about the local order and then see how well it is possible to fit the diffraction data with these different assumptions.

Three cases spanning more than 20 years of neutron and x-ray diffraction will be examined here. The first example concerns liquid Ni and the reported observation of icosahedral order in the supercooled liquid [8, 9]. Using EPSR it is possible to vary the minimum distance that two Ni atoms are allowed to approach one another. As will be seen later, it is proposed that a significant feature of both neutron and x-ray datasets is the requirement to have a relatively soft repulsive potential between Ni atoms at short distances. With this feature of the effective interatomic potential it is possible to achieve accurate reconstructions of both x-ray and neutron data, without recourse to an icosahedral model.

The second example concerns a much earlier study of vapour deposited amorphous Ge [10]. The interest in amorphous Ge is its apparent strong ability to form a tetrahedral structure in the glassy state, which, however, is significantly broken down in the liquid [11], leading to a markedly higher atomic number density in the liquid compared to the glass. Here we find it is possible to produce two structurally quite distinct models of the glass which fit the diffraction data equally well. Fortunately it is possible to exclude one of these models as being implausible in that it does not satisfy the requirement for tetrahedral local order, but the ambiguity does reveal how much the interpretation of diffraction data depends on having access to additional information about the material in question.

The final example concerns the more recent study of $GeSe_2$ in the glass state [12]. In this case the interesting question is the extent to which so-called 'homopolar' bonds exist in the glass—these are instances where pairs of Ge–Ge or Se–Se atoms approach one another as closely as Ge–Se pairs. Given the proximity of these two elements in the periodic table, and given the fact that both Ge and Se form short distances in the pure liquid or glass states [11, 13], it would perhaps not be surprising if such like–like pairing did exist in the alloy to some extent. The analysis presented in [12], which clearly affirms the existence of homopolar bonds in the glass based on the isotope substitution diffraction data presented, also discusses the controversy surrounding such bonds since it would preclude the random network model which is often invoked for such glasses. First-principles simulations of liquid $GeSe_2$ also seem to indicate significant numbers of Ge–Ge (10%) and Se–Se (39%) homopolar bonds [14]. An important factor, however, is the weak contribution that the Ge–Ge partial structure makes to the total neutron diffraction patterns. This, it is shown here, introduces significant uncertainty in extracting this function precisely from the data.

It has been verified several times [15–17] that if the forces between atoms are purely pairwise additive then there should be a unique relationship between the pair potential and all higher body correlation functions. This raises two issues, however. First it is unlikely that in real systems the forces are truly pairwise additive—three-body and higher order forces are likely to occur in most condensed phase systems. The question is how significant are they, and can they be replaced by an effective pairwise interaction? If the latter, does this ensure that the many-body correlations derived from this effective force are correct? Since diffraction data are derived from a linear transformation of the radial distribution functions, their information content is purely pairwise additive. Hence there is a significant possibility, if many body forces are present, that we may generate a structure which is consistent with the data but which has the incorrect many-body structure. There may therefore be several or an ensemble of structures which are consistent with a given diffraction dataset. Without additional many-body information it may not be possible to distinguish between these structures.

A second feature of the diffraction experiment is that even if the use of an effective pairwise additive potential is acceptable, what *sensitivity* do the data have to the details of that potential? The relationship between pairwise potential and structure may be unique, but this says nothing about sensitivity. Hence a significant change to the potential or radial distribution functions might make only an imperceptibly small change to the calculated diffraction data within errors.

Both aspects are covered in the analyses presented here. The example of amorphous Ge explores the role of many-body forces in controlling the structure, while the other two examples of liquid Ni and amorphous $GeSe_2$ demonstrate the lack of sensitivity of the data to some aspects of the interaction potential and radial distribution functions. An important feature of the present study is that by using an objective and quantitative measure of the quality of fit to the data, χ^2, one is hoping to reduce the possibility of bias being introduced by experimenters into the interpretation of their data. Certainly χ^2 is not an infallible measure of the quality of fit, particularly if there are systematic errors in the data, but it is independent of any physical constraints that may be imposed on the atomic distribution and in that sense can be used objectively to assess the reliability of one set of physical constraints against another.

In all three cases, the diffraction data have either been supplied by the relevant authors (neutron liquid Ni data [8]), or by digitizing the appropriate published graphs [9, 10, 12] when the original data could not be retrieved. In all cases the quality of the extracted data was excellent and allowed the analysis to proceed as described.

2. Details of simulations

The EPSR method has been extensively described elsewhere [7], and so it will only be summarized here. At the heart of the method is a reference potential which is used to seed the computer simulation prior to any data being introduced. This reference potential typically will contain a Lennard-Jones potential to represent dispersion forces, a Coulomb potential to represent charged atom interactions and a soft repulsive exponential potential which incorporates prior information about minimum allowed distances between atoms:

$$U_{\alpha\beta}^{(\mathrm{ref})}(r) = 4\varepsilon_{\alpha\beta}\left[\left(\frac{\sigma_{\alpha\beta}}{r}\right)^{12} - \left(\frac{\sigma_{\alpha\beta}}{r}\right)^{6}\right] + \frac{q_\alpha q_\beta}{4\pi\varepsilon_0 r} + C_{\alpha\beta}\exp\left(\frac{1}{\gamma}(r_{\alpha\beta} - r)\right) \tag{1}$$

where the value of $C_{\alpha\beta}$ is adjusted iteratively so that there are no pairs of atoms of type α, β at separations of $r < r_{\alpha\beta}$. The hardness of this repulsive term is controlled by the value of γ. The values of $\varepsilon_{\alpha\beta}$ and $\sigma_{\alpha\beta}$ control the depth and range, respectively, of the Lennard-Jones potential between atom pair (α, β), while q_α is an effective charge on atom α.

The diffraction data are introduced to the structure refinement simulation via the so-called 'weights' equations [7]:

$$D_i(Q) = \sum_{j=1,N} w_{ij} H_j(Q) \tag{2}$$

where $D_i(Q)$ represents the ith set of data, the index j runs over the N partial structure factors in the system, and the weights matrix, w_{ij}, is given for neutrons by $w_{ij} = (2 - \delta_{\alpha\beta})\, c_\alpha c_\beta \langle b_\alpha^{(i)} \rangle \langle b_\beta^{(i)} \rangle$, where j runs over all the N pairs of α, β values, and for x-rays by

$$w_{ij} = \frac{(2 - \delta_{\alpha\beta})\, c_\alpha c_\beta f_\alpha(Q) f_\beta(Q)}{(\sum_\alpha c_\alpha f_\alpha(Q))^2}.$$

A set of such weights is defined for each of M sets of measured diffraction data. In general there are fewer sets of data than partial structure factors, $M < N$, so inversion of the weights matrix is indeterminate. However, as pointed out in [7], even when $M \geqslant N$ one does not necessarily want to rely totally on the data since they will often contain systematic error which has the possibility of introducing artefacts into the simulated structure. Thus it was proposed to use the simulation itself as a type of additional dataset so that the weights matrix can be inverted under all circumstances. This was done by means of a 'feedback' factor, f, such that for the data a modified set of weights are defined, namely $w'_{ij} = f w_{ij}$, for $1 \leqslant i \leqslant M$, and $w'_{ij} = (1 - f)\delta_{(i-M),j}$; for $M < i \leqslant (M + N)$, giving rise to an overdetermined weights matrix. The value of f lies in the range $0 < f < 1$.

The inverse of this matrix, w_{ji}^{-1}, is found by least squares by requiring that the $(M + N) \times (M + N)$ matrix formed from $P_{ii'} = (\sum_{j=1,N} w'_{ij} w_{ji'}^{-1} - \delta_{ii'})$ has a minimum norm. Note that with the definitions used here and provided $f < 1$, an inverse of this modified weights matrix can always be found. As f approaches unity the emphasis on the data increases, along with the increasing risk of artefacts being introduced into the reconstructed structure. As f is made smaller the risk of artefacts decreases, but so does the ability to fit the data. Hence a value which minimizes the artefacts but gives best fit to the data has to be chosen, usually by inspection. For all the cases discussed in this paper the feedback factor was set between 0.8 and 0.9, the precise value within this range not being important to the final outcome [7].

Using the inverse of this matrix, the perturbation to the jth interatomic potential that is needed at each iteration of the algorithm is estimated from:

$$\Delta U_j(r) = \text{Fourier transform of } \left\{ \sum_{i=1,M} w_{ij}^{\prime -1} (D_i(Q) - F_i(Q)) \right\}, \qquad j = 1, N, \tag{3}$$

where $D_i(Q)$ is the ith diffraction dataset, and $F_i(Q)$ is the fit to those data derived from the simulation. These perturbations, when accumulated, form the empirical potential which is used in conjunction with the reference potential to drive the simulation. The method of performing the Fourier transform, which must avoid introducing spurious structure into the interaction potential if at all possible, is described in detail elsewhere [7]. In order to prevent artefacts from the data from being transferred to the simulation the amplitude of the empirical potential defined by

$$\bar{U} = 4\pi\rho \sum (2 - \delta_{\alpha\beta})\, c_\alpha c_\beta \int r^2 |U_{\alpha\beta}(r)| g_{\alpha\beta}(r)\, \mathrm{d}r \tag{4}$$

is limited to a specified value. The larger this value then the better the fit to the data, but it then carries the risk of introducing artefacts from the data that have nothing to do with the true structure. The quality of fit to the ith dataset is defined by the quantity

$$\chi^2(i) = \frac{1}{n_Q(i)} \sum_Q (D_i(Q) - F_i(Q))^2 \tag{5}$$

Table 1. Parameters used in the simulation of liquid Ni using single atoms. All simulations were performed at 1435 K. The values of $C_{\alpha\beta}$ are indicative as they can vary as the simulation proceeds, depending on the extent to which the given atom pair proceeds below the specified minimum separation.

Simulation	No. of atoms	Box size (Å)	$\varepsilon_{\mathrm{NiNi}}$ (kJ mol^{-1})	σ_{NiNi} (Å)	C_{NiNi} (kJ mol^{-1})	r_{NiNi} (Å)	γ (Å)	χ^2 (neutron data)	χ^2 (x-ray data)
100	2048	28.9627	0.01	1.0	3.0	1.00	0.5	0.0022	0.0048
130	2048	28.9627	0.01	1.0	14.9	1.30	0.5	0.0022	0.0036
160	2048	28.9627	0.01	1.0	24.7	1.60	0.5	0.0029	0.0030
190	2048	28.9627	0.01	1.0	41.2	1.90	0.5	0.0051	0.0039

Table 2. Parameters for the soft repulsive core in the second amorphous Ge simulation. As with table 1, the values of $C_{\alpha\beta}$ are indicative as they can vary as the simulation proceeds.

C_{Ge1Ge1} (kJ mol^{-1})	r_{Ge1Ge1} (Å)	C_{Ge1Ge2} (kJ mol^{-1})	r_{Ge1Ge2} (Å)	C_{Ge2Ge2} (kJ mol^{-1})	r_{Ge2Ge2} (Å)
0.74	3.2	0.07	2.2	0.74	3.20

where $n_Q(i)$ is the number of Q values in the ith dataset. A mean value of χ^2 is defined as $\chi^2 = \frac{1}{M}\sum_i \chi^2(i)$.

2.1. Liquid Ni simulations

For liquid Ni a set of four EPSR simulations was completed. For the different simulations, each of which consisted of 2048 individual Ni atoms in a cubic box of dimension 28.9627 Å, four different values of r_{NiNi} (equation (2)) were used, namely 1.0, 1.3, 1.6 and 1.9 Å. Table 1 lists the parameters of the reference potentials for these simulations. In all cases the simulations were started from a completely random set of atom positions within the box.

2.2. Amorphous Ge simulations

For amorphous Ge two simulations were performed. In the first simulation (a) a single type of Ge atom was allowed in the box. The Ge atoms (numbering 2000) were contained in a box of dimension 36.9174 Å, giving rise to the reported number density of 0.039 75 atoms Å^{-3} [10]. The Lennard-Jones parameters were 0.2 kJ mol^{-1} and 2.0 Å for ε and σ, respectively, and the minimum separation in the reference potential was set to 2.2 Å, with the hardness parameter, γ, set to 0.3 Å.

The second simulation (b) contained two types of Ge atoms, Ge1 and Ge2, in equal quantities with the same overall atomic number density and the same Lennard-Jones and charge parameters for both Ge1 and Ge2 as for simulation (a). The parameters for the repulsive term of the reference potential for this second simulation are given in table 2, and the hardness parameter, γ, was the same as for simulation (a). Note that Ge1 and Ge2 are distinguished by the assumed minimum distance, which for both Ge1–Ge1 and Ge2–Ge2 pairs was set to 3.2 Å, while for Ge1–Ge2 pairs the minimum distance was set to 2.2 Å. This means that each Ge1 atom can only be surrounded by Ge2 atoms at short distance, and vice versa. This was a device used to form only tetrahedral-like structures around each Ge atom in the simulation, a feature which was not enforced in simulation (a).

Table 3. Parameters for the soft repulsive core in the $GeSe_2$ simulations. The value of γ was held at 0.2 Å throughout. As with table 1, the values of $C_{\alpha\beta}$ are indicative as they can vary as the simulation proceeds. Also shown is the value of χ^2 for the different simulations.

Simulation number	Simulation name	C_{GeGe} (kJ mol^{-1})	r_{GeGe} (Å)	C_{GeSe} (kJ mol^{-1})	r_{GeSe} (Å)	C_{SeSe} (kJ mol^{-1})	r_{SeSe} (Å)	χ^2 ($\times 10^{-3}$)
1	2020	0.5	2.0	0.6	2.0	∼0.0	2.0	0.225
2	2222	0.1	2.2	0.6	2.0	∼0.1	2.2	0.231
3	2424	∼0.0	2.4	0.4	2.0	2.0	2.4	0.427
4	2626	∼0.1	2.6	0.3	2.0	1.1	2.6	0.500
5	2828	0.2	2.8	0.3	2.0	0.5	2.8	0.532
6	3030	0.2	3.0	0.1	2.0	0.4	3.0	0.605
7	2026	0.1	2.0	0.1	2.0	0.5	2.6	0.501
8	2220	0.1	2.2	0.2	2.0	∼0.0	2.0	0.194
9	2420	0.2	2.4	0.2	2.0	∼0.0	2.0	0.207
10	2620	0.1	2.6	0.1	2.0	∼0.0	2.0	0.202
11	2820	0.1	2.8	0.1	2.0	0.1	2.0	0.225
12	3020	0.1	3.0	0.1	2.0	0.1	2.0	0.258

2.3. Amorphous $GeSe_2$ simulations

For all the amorphous $GeSe_2$ simulations reported here, the Lennard-Jones parameters for both Ge and Se were set to 0.1 kJ mol^{-1} for ε and 2.0 Å for σ. The number of atoms in the simulation box was 3000 and the box dimension was 44.7842 Å. All control of the near neighbour separations was achieved via the soft repulsive exponential potential, with a hardness parameter of 0.2 Å used throughout. The values of the minimum distances used are given in table 3.

It will be seen that in all the simulations the value of r_{GeSe} is held constant at 2.0 Å. For simulations 1–6, the values of r_{GeGe} and r_{SeSe} are the same and increase from 2.0 to 3.0 Å. For simulation 7 r_{GeGe} is held at 2.0 Å, i.e. the same value as simulation 1, while r_{SeSe} is set to 2.6 Å. For simulations 8–12 r_{SeSe} is held constant at 2.0 Å as in simulation 1, while r_{GeGe} increases systematically to 3.0 Å.

3. Results and discussion

3.1. Liquid Ni

Figure 1 shows the mean χ^2 for the joint fits to the neutron [8] and x-ray [9] diffraction data for supercooled liquid Ni at ∼1435 K (1490 K for the x-ray data) as a function of the minimum separation. It is clear that the best fits are obtained with the shorter minimum separations between Ni atoms. Figure 2 shows the radial distribution functions obtained from the two best fits with r_{NiNi} at 1.3 and 1.6 Å, respectively. These extracted $g(r)$s clearly show extra intensity on the low r side of the first peak. In fact the original papers [8, 9] also show this extra low r intensity, but it is not commented on. For $r_{NiNi} = 1.6$ Å the extra intensity appears as a soft edge on the main peak while at $r_{NiNi} = 1.3$ Å it appears as a separate peak. This separate peak may be a consequence of the way the empirical potential is represented by Poisson functions [7], but it nonetheless reflects the need from some extra intensity at short distances based on the published data. The number of Ni atoms in this peak is quite small, approximately 0.3 atoms, compared to a coordination number of ∼13 in the main peak; that is it represents only ∼2% of the main peak coordination number.

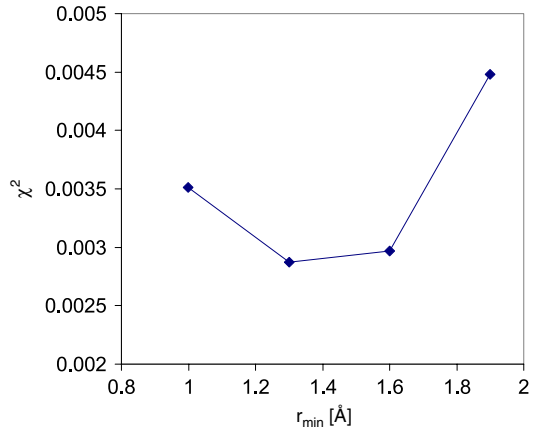

Figure 1. Values of χ^2 for the different EPSR simulations of the neutron and x-ray diffraction data from supercooled liquid Ni at 1435 K (1490 K for the x-ray data).

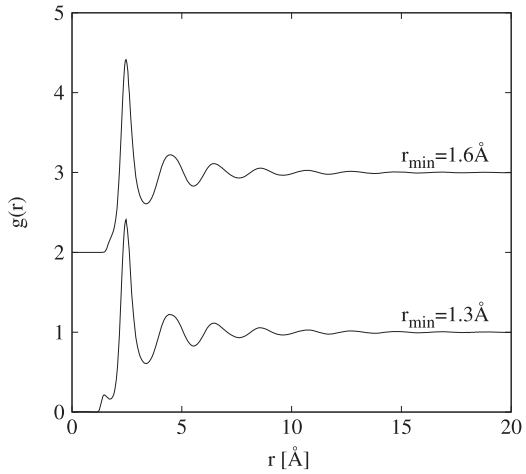

Figure 2. Radial distribution functions for liquid Ni extracted by EPSR analysis of x-ray [9] and neutron [8] diffraction data taken 1435 K (1490 K for the x-ray data). The best two fits to the data are shown (figure 1 and table 1).

Ignoring the higher frequency truncation oscillations at low Q, which arise from the finite box size used in the simulation, we see from figure 3 that the fits give an accurate account of the diffraction data. In particular it is interesting to note that the fits capture the measured shape of the second diffraction peak quite accurately. The shape of this peak has been used to argue that the structure of supercooled liquid nickel can be understood in terms of local icosahedral order [8, 9]. Based on the present results, however, an alternative explanation for the shape of this peak can be advanced, in that the shape is only accurately captured by the simulation when a soft repulsive core is allowed in the simulation. We hope to report a more detailed analysis of this effect in the near future.

It could be argued of course that the low r intensity seen in these EPSR simulations is purely an artefact of the diffraction data, such as a normalization error in the data analysis

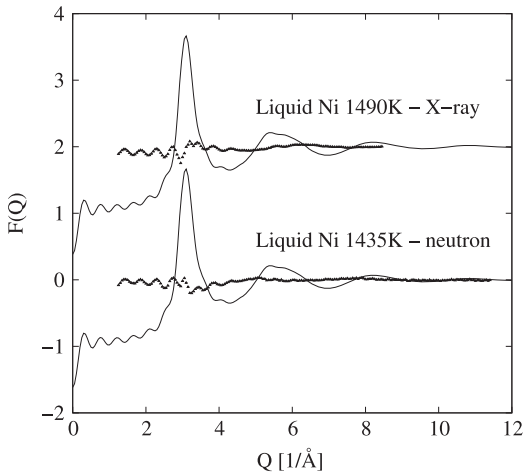

Figure 3. EPSR fits to the neutron and x-ray diffraction data from supercooled liquid Ni at 1435 K (1490 K for the x-ray data) for $r_{\mathrm{NiNi}} = 1.6$ Å. The line shows the EPSR fit, while the dots show the residual between the data and the fit. Truncation oscillations are seen up to $Q \sim 5.0$ Å^{-1}, and are believed to be caused by the finite size of the box used in these simulations.

procedures. If this were so, it would seem surprising that exactly the same error occurs for both the neutron and x-ray diffraction data, since the data analysis procedures would be quite different for the two datasets, with strongly Q-dependent form factors for the x-ray data and marked Compton scattering, compared to the Q-independent form factors and nearly flat background for the neutron data. Further evidence for this low r intensity comes from earlier neutron diffraction and x-ray levitated sample data [18, 19] where in both cases there seems to be a small amount of low r intensity. Moreover introducing the low r intensity into the EPSR simulation appears to be an important prerequisite to obtaining a satisfactory fit to the *shape* of the second diffraction peak. On the other hand some experts might object to the notion of Ni atoms approaching each other so closely. This analysis therefore serves to highlight the difficulty of extracting reliable structure information from diffraction data.

3.2. Amorphous Ge

Figure 4 shows the fits to the amorphous Ge diffraction data for both of the proposed models and the residuals between fit and data. It can be seen that both models give an accurate account of the data and that they are to a very large extent indistinguishable. The value of χ^2 for simulation (a) was ∼0.000 82 and for simulation (b) 0.000 85, which confirms this view. (It is worth mentioning here that one of the authors of the original paper [10], Wright, has pointed out in a private communication that the amorphous Ge used in the diffraction experiment may have been contaminated with water or hydrogen, giving rise to local structural defects. This fact, however, does not affect the primary conclusions of the present paper which are to do with how well we know the structure of a disordered material based on a set of diffraction data.)

It is also possible to compare the radial distribution functions for the two models. To do this for the second model, which involves two types of Ge atom, the average radial distribution function was formed:

$$g_{\mathrm{GeGe}}(r) = \tfrac{1}{4}(g_{\mathrm{Ge1Ge1}}(r) + 2g_{\mathrm{Ge1Ge2}}(r) + g_{\mathrm{Ge2Ge2}}(r)) \tag{6}$$

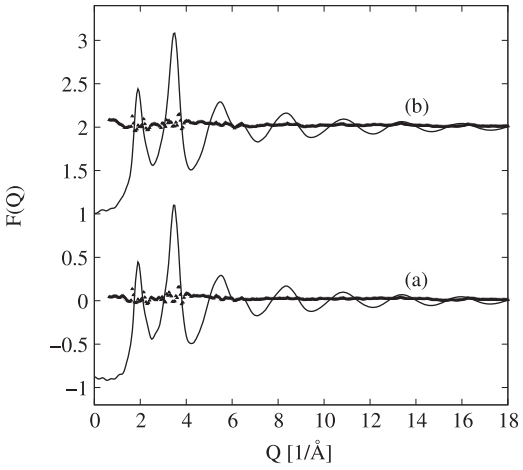

Figure 4. EPSR fits to the neutron diffraction data for amorphous Ge [10]. For simulation (a) the Ge atoms are treated as identical, while for simulation (b) the Ge atoms are split into two kinds, Ge1 and Ge2, as described in the text and table 2. Both simulations have the same fitting parameter, $\chi^2 = 0.001$.

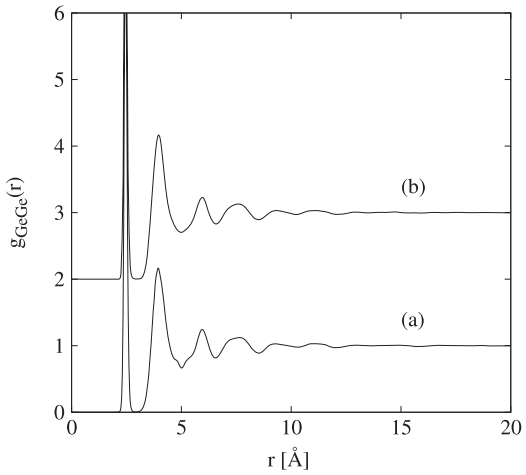

Figure 5. Radial distribution functions for amorphous Ge, from the EPSR simulations shown in figure 4 and described in the text. For (b) the average radial distribution function as defined by equation (6) is shown. The differences between these two $g(r)$s are indistinguishable in the data, figure 4.

This comparison is shown in figure 5, where it is revealed that in r-space the two radial distribution functions are also almost identical, barring some very small differences near $r = 5$ Å.

Despite the almost identical fits to the diffraction data, the structural difference between the two models is strikingly captured in the so-called 'bond angle' distribution function, $p(\theta)$ (figure 6). For simulation (a) a bond is defined if two Ge atoms are within 3.0 Å of each other. For simulation (b) a bond is defined if a Ge1 and a Ge2 atom are within 3.0 Å of each other. The simulation box is then searched for triplets of Ge atoms at least two pairs of which are bonded. The included angle θ between the two bonds is calculated for the atom common to both bonds.

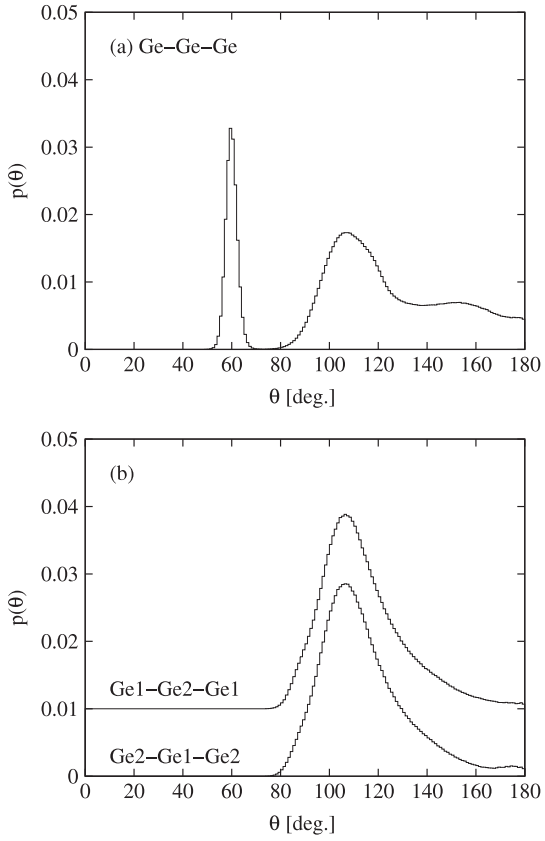

Figure 6. Bond angle distribution functions for amorphous Ge, as described in section 3.2. A bond between two Ge atoms is defined to exist if their separation is 3.0 Å or less. For simulation (b) there are two distributions to show, namely Ge1–Ge2–Ge1 and Ge2–Ge1–Ge2, but as can be seen they are essentially the same. The distribution functions have been normalized to the sin θ distribution that would occur if the bond angles occurred at random.

The distribution of these angles is then normalized to the distribution that would occur if the bond angles were randomly distributed, namely $\sin\theta$. For simulation (a) there is only one bond angle distribution to show, namely that formed by Ge–Ge–Ge triplets, but for simulation (b) there are two such distributions to show, namely for Ge1–Ge2–Ge1 and Ge2–Ge1–Ge2 triplets. For simulation (a) the bond angle distribution has a sharp peak at $\sim$60° indicating that equilateral triangles of Ge atoms are occurring throughout the simulation box. Such equilateral triangles are not permitted if Ge forms primarily a tetrahedral environment about itself. Note that there is also a broader distribution near the tetrahedral angle, 109.47°, indicating that some Ge atoms do form local tetrahedral-like environments in this case. For simulation (b) there is only a pronounced distribution around the tetrahedral angle, for both types of triplets, indicating that this model has indeed forced a primarily tetrahedral local environment on the model, irrespective of whether a Ge1 or Ge2 atom is at the origin.

We have here an example of two rather different local structures both being equally compatible with a set of diffraction data. The only way to distinguish between the models is to impose additional information, namely that we expect the Ge environment to be predominantly tetrahedral-like. Without that extra information there is no way of saying which model is

correct. This is a clear example of recent literature studies that the pair correlation function does not contain all the local structure information on a system [20]. An important consequence of this result is that one has to be very careful about the structural interpretation of a set of diffraction data: there may be a model out there that we have not thought of which fits the data perfectly well. Unless we have clear additional indications that such a model is physically not allowed, then it has to be included in our assessment of the structure, and this gives us the potential problem of trying to determine which of all possible structural models can be included. This is a much larger topic than can be addressed satisfactorily here.

3.3. Amorphous $GeSe_2$

The present study of existing neutron diffraction data on amorphous $GeSe_2$, in which Ge and Se isotope substitution had been performed to extract the GeGe, GeSe and SeSe partial structure factors [12], was prompted by the *ab initio* simulation work of Massobrio *et al* [14] in which a significant number of homopolar bonds appeared in the simulation. The question was: is it possible to say for sure whether such homopolar bonds can be sustained on the basis of the diffraction data? The original analysis [12], and indeed the previous analysis of the liquid diffraction data [11], strongly hinted that such bonds do exist in the liquid and glassy forms, but the coordination numbers were quite small (∼0.2 for both GeGe and SeSe). The purpose of the EPSR simulations described in section 2.3 and table 3 was to address this question by choosing different minimum separations for the Ge–Ge and Se–Se pairs and to see whether restricting these minimum separations to distances outside the homopolar bond distance range would tangibly affect the quality of the fit to the data. Table 3 also shows the fit parameters for all these simulations.

Figure 7(a) shows the best fit to the data, simulation number 8, where $r_{\mathrm{GeGe}} = 2.2$ Å and $r_{\mathrm{SeSe}} = 2.0$ Å. The fits appear to be remarkably good, which attests to the extremely high quality of the original data. Figure 8 (solid lines) shows the site–site radial distribution functions which correspond to this fit, and we can see immediately that there are indeed significant homopolar bonds for both the Ge–Ge and Se–Se distribution functions. Integrating these functions out to the first minimum in the Ge–Se distribution function at 2.73 Å it is found there are ∼0.6 atoms of Ge around Ge, ∼3.3 atoms of Se around Ge and ∼0.3 atoms Se around Se at this distance. In other words approximately 15% of the atoms in the first neighbour shell of Ge are in fact Ge atoms. Hence the Ge atom appears to be four-fold coordinated as might be expected for this network glass, but with a significant fraction of that coordination shell consisting of like atoms.

How reliable are these conclusions? Table 3 gives the clue. First consider simulations 1–6 where the minimum distance for both Ge–Ge and Se–Se is systematically increased from 2.0 to 3.0 Å in steps of 0.2 Å. It can be seen that for simulations 1 and 2 the quality of fit is similar, but from simulation 3 onwards the fit gets progressively worse, implying that the data do require short Ge–Ge and Se–Se distances in order to be fit satisfactorily.

The next question then is: which of these pairs is important, or are they both important? Simulation 7 indicates part of the answer. Here the Ge–Ge minimum distance has been left at 2.0 Å, but the Se–Se minimum distance set to 2.6 Å. The quality of fit is the same as simulation 4 where the Ge–Ge minimum distance was also set to 2.6 Å, but it is also 2.5 times worse than the best fit, simulation 8. Therefore it seems that homopolar Se–Se distances are a fundamental requirement if the diffraction data are to be understood.

The effect of varying the minimum Ge–Ge distance is determined from simulations 1 and 8–12. In these simulations the minimum Se–Se distance is held fixed at 2.0 Å, while the Ge–Ge minimum distance is increased from 2.0 to 3.0 Å in steps of 0.2 Å. Now we see a much *slower*

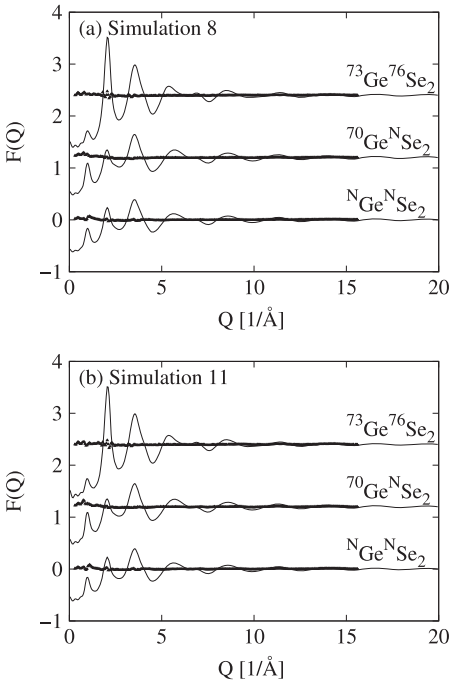

Figure 7. EPSR fits to the isotope substituted neutron diffraction data for amorphous $GeSe_2$ [12], for simulation 8(a) (the best fit) and simulation 11(b) (see table 3). The superscripts refer to the nominal isotope composition of each component, with 'N' representing the naturally occurring isotopic composition. The precise composition of each sample is given in the original reference [12]. The data have been offset vertically for clarity. The lines show the EPSR simulated diffraction data, and the points represent the residual between data and fit.

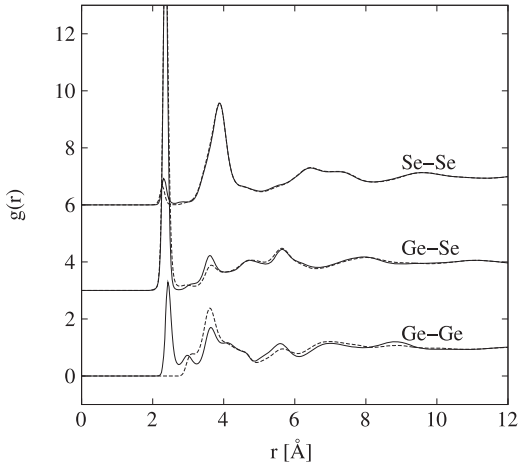

Figure 8. Comparison of site–site radial distribution functions for amorphous $GeSe_2$ as obtained from EPSR simulation 8 (solid line) and simulation 11 (dashed line). The difference in fitting parameter for these two simulations is ∼16% (see table 3) indicating that the data are relatively insensitive to the precise details of the Ge–Ge distribution function, while the Se–Se and Ge–Se distributions are quite well constrained by the data.

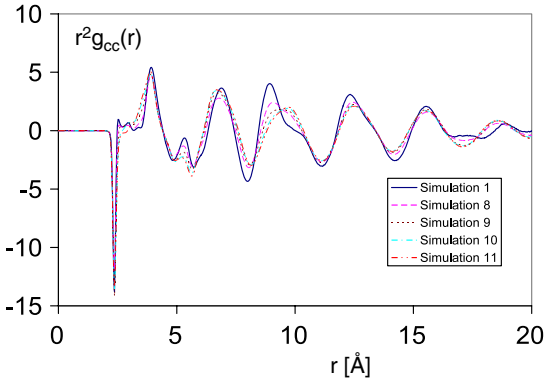

Figure 9. Bhatia–Thornton concentration–concentration correlation function, $g_{CC}(r)$, for amorphous $GeSe_2$ as determined from the different EPSR simulations of this material. See legend and table 3 for details of the different simulations.

variation in the value of χ^2 with change in minimum Ge–Ge distance, the variation being only about 30% over the full distance range. This compares markedly with the drastic change of fit parameter as the Se–Se minimum distance was varied. There is a strong indication here that the diffraction data are far less sensitive to the Ge–Ge distribution than to the Ge–Se and Se–Se distributions. This is borne out by the relatively small contribution made by the Ge–Ge distribution to any of the diffraction datasets [12].

Figure 7(b) shows the fit for simulation 11 where the value χ^2 has worsened by ∼16% compared to the best fit simulation 8. The difference in quality of the two fits is barely visible on the scale of the plots and the likely uncertainties. Figure 8 compares the radial distribution functions for these two cases. It is clear that significant uncertainties in the Ge–Ge distribution can arise, even when the Ge–Se and Se–Se distributions are better defined, and even with the extremely high quality data that are available in this case. One particular feature we can see is that a relatively small change in $g_{GeSe}(r)$ between the two fits near $r \sim 3.5$ Å is compensated for by a much larger change in $g_{GeGe}(r)$ at the same r value, while $g_{SeSe}(r)$ is barely altered in this region. This symbiotic relationship between the different site–site $g(r)$s which contribute to a diffraction dataset is rarely referenced when assessing the errors in these functions extracted from experiment.

As a final endnote to this section, the work of Salmon *et al* [21] has highlighted the similarity of the local and longer range order in different tetrahedral glasses with different interatomic forces, and also the fact that the Bhatia–Thornton [22] (BT) number–number and concentration–concentration distribution functions are important for discussing this order. If there is uncertainty in one or more of the site–site distribution functions, then this in turn will affect the extracted BT distribution functions. To show this uncertainty in the present instance, the different BT concentration–concentration distribution functions, $r^2 g_{CC}(r)$, for simulations 1 and 8–11 are shown in figure 9. For these five simulations the fit parameter varies by less than 16%, yet the changes in the concentration–concentration correlation are quite marked, particularly in the intermediate distance range near ∼10 Å. Note that the variations at short distance in this function are much less marked than at longer distances, indicating that changes in the local order around the Ge atoms in this material have a marked impact on the longer range concentration–concentration fluctuations. Variations in the number–number and number–concentration correlation functions between the different simulations are much less marked, and are not shown here.

Comparing the present $g(r)$s for amorphous $GeSe_2$ with those shown in the original publication [12], there are many similarities but some dissimilarities also, particularly in the GeGe functions. For example in both cases the SeSe homopolar peak is at a shorter distance than the corresponding GeGe homopolar peak, while the main SeSe peak near 4 Å is at a longer distance than the corresponding GeGe peak near 3.5 Å. On the other hand the shape of the GeGe distribution is quite different in the two analyses and even changes a lot between simulations 8 and 11, in spite of both simulations giving a good account of the data (figure 7). The uncertainty in the GeGe function seen here is indicative of the uncertainties that diffraction experiments contain, particularly when one (or more) contributions to the diffraction data is only weakly weighted. In the present instance the relative weighting on the GeGe partial structure factor in the total diffraction pattern varies from ∼3% for the dataset labelled '7376' to ∼15% for the dataset labelled '70N', being ∼12% in the dataset labelled 'NN'. Thus in no dataset does the GeGe distribution make a significant contribution, which presumably explains the current uncertainties. It is not clear how these uncertainties can be removed without additional constraints being imposed on the local structure around Ge.

4. Summary and conclusion

By looking at EPSR simulations of three different diffraction datasets on supercooled liquid Ni, amorphous Ge and amorphous Ge Se_2 it has been shown here that marked differences in the local order of a liquid or glassy solid can be extracted from the data depending on the precise initial assumptions that are made about the forces between atoms. In the case of liquid Ni there was uncertainty about what minimum distance to choose, but a clear indication that in order to fit the shape of the second diffraction peak it was necessary to allow a small amount (∼2%) of low r intensity. This observation may have ramifications for the purported icosahedral order observed in these supercooled melts [8, 9].

For amorphous Ge two distinct structural models could be found which gave equally good fits to the available diffraction data. Albeit the sample used in this experiment may be contaminated, the fact remains it is not possible to distinguish between the models without imposing additional, many-body, constraints on the model beyond those supplied by the diffraction data.

In amorphous $GeSe_2$ it was seen that there is clear evidence that Se–Se homopolar bonds do occur in this material. The data are of an extremely high quality in this case; nonetheless some variations in the acceptable structures were observed, particularly as regards the Ge–Ge radial distribution function, which does not appear to be well constrained by the data. What is observed however is that as $g_{GeGe}(r)$ varies between the different simulations there are compensating, but much smaller, changes in $g_{GeSe}(r)$ and almost none in $g_{SeSe}(r)$, giving a clear idea of where the uncertainties in the experiment lie. There remains some uncertainty as to whether homopolar Ge–Ge bonds are present or not. The best fit model implies they are present at the level of ∼15% compared to Ge–Se correlations at the same distance, but variations down to 0% Ge–Ge homopolar bonds are possible without compromising the quality of fit appreciably. Moreover uncertainties in the local environment of Ge in this material have a marked impact on the Bhatia–Thornton concentration–concentration correlation function at longer distances.

Based on the above analyses it should now be clear that interpreting diffraction data in terms of radial distribution functions and three-dimensional structures is a highly non-trivial process. In the case of liquid Ni and amorphous $GeSe_2$ it appears there are significant uncertainties on the precise forms of the radial distribution functions that can be derived from the diffraction data. For amorphous Ge it was possible to generate two almost identical radial

distribution functions which produced equally good fits to the diffraction data, but which however had two quite different underlying three-dimensional structures. These cases highlight the joint difficulties of extracting reliable radial distribution functions from diffraction data in the first place, and subsequently attempting to understand that radial distribution function in terms of a three-dimensional structure. This is not the first time that these difficulties have been alluded to, but with the present approach using EPSR it seems there is real chance to identify and quantify in a relatively objective manner which parts of a given interpretation are reliable and which are not. Relying solely on the Fourier transform of the diffraction data gives us little idea of what confidence we should attribute to any structural conclusions we might come to.

There clearly is much scope still to improve the EPSR method itself, to introduce a broader range of reference potentials, and in particular to introduce some form of realistic many-body (particularly triple-body) potential, in order to enable the range of possible structures against which the data can be tested to be significantly widened. Work on this is currently in progress. In the meantime for the purposes of comparing the results of diffraction experiments with other techniques such as computer simulation it will be important, if not essential, to first assess the reliability of radial distribution functions and other structural parameters obtained from the experiment. The present work is not comprehensive in this regard, but it does give a strong hint that checking the reliability of the interpretation of the data should be a fundamental aspect of any structural enquiry.

Acknowledgment

I am indebted to Franz Demmel for drawing my attention to the problem of icosahedral order in liquid Ni.

References

[1] Schommers W 1983 *Phys. Rev.* A **28** 3599–605
[2] Levesque D, Weis J J and Reatto L 1985 *Phys. Rev. Lett.* **54** 451–4
[3] McGreevy R L and Pusztai L 1988 *Mol. Simul.* **1** 359
[4] McGreevy R L 2001 *J. Phys.: Condens. Matter* **13** R877–913
[5] Neuefeind J, Fischer H E and Schröer W 2000 *J. Phys.: Condens. Matter* **12** 8765–76
[6] Tóth G 2001 *J. Chem. Phys.* **115** 4770–5
[7] Soper A K 2005 *Phys. Rev.* B **72** 104204
[8] Schenk T, Holland-Moritz D, Simonet V, Bellissent R and Herlach D M 2002 *Phys. Rev. Lett.* **89** 075507
[9] Lee G W, Gangopadhyay A K, Kelton K F, Hyers R W, Rathz T J, Rogers J R and Robinson D S 2004 *Phys. Rev. Lett.* **93** 037802
[10] Etherington G, Wright A C, Wenzel J T, Dore J C, Clarke J H R and Sinclair R N 1982 *J. Non-Cryst. Solids* **48** 265–89
[11] Salmon P S 1988 *J. Phys. F: Met. Phys.* **18** 2345–52
[12] Salmon P S and Petri I 2003 *J. Phys.: Condens. Matter* **15** S1509–28
[13] Bellissent R 1982 *Nucl. Instrum. Methods* **199** 289
[14] Massobrio C, Pasquarello A and Car R 1998 *Phys. Rev. Lett.* **82** 2342–5
[15] Henderson R L 1974 *Phys. Lett.* A **A49** 197–8
[16] Gray C G and Gubbins K E 1985 *Theory of Molecular Fluids–I: Fundamentals* (Oxford: Oxford University Press)
[17] Evans R 1990 *Mol. Simul.* **4** 409–11
[18] Waseda Y 1980 *The Structure of Non-Crystalline Materials* (New York: McGraw-Hill)
[19] Krishnan S and Price D L 2000 *J. Phys.: Condens. Matter* **12** R145–76
[20] Stillinger F H and Torquato S 2004 *J. Phys. Chem.* B **108** 19589–94
[21] Salmon P S, Martin R A, Mason P E and Cuello G J 2005 *Nature* **435** 75–8
[22] Bhatia A B and Thornton D E 1970 *Phys. Rev.* B **2** 3004–12